

Mountain torques and
Northern-Hemisphere low-frequency
variability.
Part II: Regional aspects

François Lott¹, Andrew W. Robertson² and
Michael Ghil ³

Laboratoire de Météorologie Dynamique du CNRS,
Ecole Normale Supérieure

July 2, 2003: revised version.

¹Corresponding author address: Dr François Lott, LMD CNRS, ENS, 24, rue
Lhomond, 75235 PARIS Cédex 05, France. Phone: 33 (0)1 44 32 27 52; Fax: 33
(0)1 43 36 83 92; E-mail: flott@lmd.jussieu.fr

²International Research Institute for Climate Prediction, Palisades New York

³Additional permanent address: Department of Atmospheric Sciences and In-
stitute of Geophysics and Planetary Physics, UCLA

Abstract

Important aspects of low-frequency variability (LFV) are regional in character, while the mountain torques of the Rockies and the Himalayas evolve quite independently of each other. The hemispheric analysis of Part I is complemented therefore herein by an analysis of the relationships between individual mountain torques and sectorial LFV patterns in the NCEP/NCAR reanalysis.

In the 20–30-day band, relationships are found between the Rockies (Himalayas) torque and the dominant patterns of LFV over the Pacific (Eurasia). The composites of the atmospheric flow fields that accompany the Rockies (Himalayas) torque in this band exhibit similarities with known low-frequency oscillations that dominate the Pacific and North-American (European and North-Atlantic) sectors during certain winters. The composites keyed to the 20–30-day Rockies torque affect the Persistent North Pacific (PNP) pattern that controls the extension of the mid-latitude jet stream over the eastern Pacific. Furthermore, the unfiltered torques for the Northern Hemisphere (NH) and Rockies anticipate the onset of the two dominant winter Pacific circulation regimes that correlate strongly with the PNP pattern. The composites keyed to the 20–30-day Himalayas torque affect the North Atlantic Oscillation (NAO) pattern, which controls the intensity of the North-Atlantic jet stream. Furthermore, the unfiltered torques for the NH and the Himalayas anticipate the breaks of the two dominant winter Atlantic circulation regimes, which correlate strongly with the

NAO pattern.

These analyses also show that the 20–30-day Rockies (Himalayas) torques produce substantial atmospheric angular momentum (AAM) changes, which are nearly in phase with and larger in amplitude than the AAM changes associated with the mid-latitude eastern Pacific (North-Atlantic) jet stream variations seen in the composite maps. This result suggests that the Rockies (Himalayas) torque variations drive, at least partially, but actively the changes in the eastern Pacific (North-Atlantic) jet stream.

These results are consistent with the Himalayas and the Rockies torques contributing separately to changes in the two leading hemispheric EOFs that were described in Part I; the two are associated with a hemispheric index cycle and the Arctic Oscillation, respectively.

1 Introduction and motivation

In Part I of this study (Lott et al. 2003), we have shown that the atmospheric circulation patterns associated with the Northern Hemisphere (NH) mountain torque (T_M) in the 20–30-day band, have large amplitudes in well defined geographical areas of the Pacific–North-American and North-Atlantic–European sectors, located far from the major mountain ranges. These localized patterns suggest that mountain torques and low-frequency variability (LFV) may be related on a regional scale as well. A regional approach is also justified by numerous

observational (Wallace and Gutzler 1981; Penland et al. 1991; Cheng and Wallace 1993; Kimoto and Ghil 1993b; Plaut and Vautard 1994; Smyth et al. 1999) and model (Ghil et al. 1991b; Marcus et al. 1996) studies, which have shown that LFV is often regional in character.

Relationships between regional mountain torques and sectorial LFV, although not previously identified, can be expected for various reasons. In Part I for instance, the signal in 700-hPa geopotential heights (Z_{700}) that is related to the 20–30-day NH mountain torque propagates westward over the Pacific, suggesting that it is associated with the traveling low-frequency oscillations that dominate Pacific LFV during certain winters (Branstator 1987; Kushnir 1987). Other sectorial LFV patterns can generate regional mountain torques because they are strongly nonzonal and located near the dominant NH mountain ranges. They can thus induce pressure differences in the zonal direction across these ridges and therewith a mountain torque. Conversely, mountains can force Rossby lee waves that may explain blocking onset downstream of the major ridges (Kalnay-Rivas and Merkin 1981). Through interactions between traveling low-frequency oscillations and the major mountain ranges, regional mountain torques can also provide part of the force needed to change the jet stream intensity in certain regional sectors.

Observational studies that emphasize the temporal characteristics of LFV have focused on persistent and quasi-stationary flow configurations, generally called persistent anomalies (Dole and Gordon 1983). The often intermittent

nature of atmospheric LFV suggests that an alternative or complementary approach to the oscillatory description used in Part I of this paper (see also Dickey et al. 1991; Plaut and Vautard 1994; Marcus et al. 1996) is necessary (Ghil et al. 1991a; Ghil and Roberston 2002). This approach consists of (1) analyzing LFV in terms of flow regimes (Mo and Ghil 1987; Cheng and Wallace 1993; Kimoto and Ghil 1993a), and (2) describing the transitions between them (Ghil 1987; Vautard et al. 1990; Kimoto and Ghil 1993b; Koo et al. 2002).

The first purpose of Part II of this study is to examine relationships between the two major NH mountain ranges (Rockies and Himalayas) and the major patterns of regional LFV in the 20–30-day band; the importance of this band for hemispheric relationships between LFV patterns and mountain torques was demonstrated in Part I. Second, we want to verify, using atmospheric angular momentum (AAM) budgets, whether the observations confirm that regional mountain torques play an active role in driving regional LFV patterns. Third, we want to determine to what extent, if any, the results in Part I have significant regional aspects. Fourth, we want to know if these relationships are substantial enough for the individual torques to be related with sectorial weather regimes.

We pursue the investigation of the statistical relationships between NH LFV and mountain torques made in Part I by carrying out a regional analysis of LFV and mountain torques. The dataset used for these purposes is, again, the NCEP/NCAR reanalysis dataset described in Part I. To reduce the length of the series and to focus on the intraseasonal (IS), 10–150-day band, we also proceed as

in Part I (see beginning of section 2 there). and form two sets of series sampled every 3 days, the 3d series and the IS series respectively.

In section 2, we study separately the regional torques and the sectorial patterns of NH LFV. In section 3, we analyze the relationships between the Rockies torque and the Pacific–North–American variability. section 4 deals with the relationships between the Himalayas torque and the variability over the Atlantic–European and Eurasian sectors. In section 5, we study sectorial LFV in terms of multiple circulation regimes, and investigate the relationship, if any, between regional mountain torque anomalies and these regimes. The conclusions of Part II follow in section 6.

2 Regional analysis: torques and EOFs

a. Regional torques

Figure 1

Figure 1 shows the 3d-series of the NH mountain torque T_M and the individual contributions of the Rockies and Himalayas to that torque over the same 13-month interval as in Fig. 1 of Part I. The Rockies and Himalayas torque in Fig. 1 are evaluated using Eq. (7) in Part I, but with the sum limited to the domains $(160^\circ\text{W}–85^\circ\text{W}, 20^\circ\text{N}–70^\circ\text{N})$ and $(55^\circ\text{E}–125^\circ\text{E}, 20^\circ\text{N}–35^\circ\text{N})$, respectively. The dominant contribution to the NH torque over the entire 40-year interval comes from the sum of the torques due to the Rockies and the Himalayas (not shown). The variance of the sum of these two torques represents 85% of the

variance of the entire NH torque. The two regional torques have comparable amplitude, the variance of the Rockies torque being 75% of the Himalayas’.

The Himalayas and Rockies torques evolve quite independently of each other: the correlation between the two is 0.1 for the 3d series and 0.05 for the IS series. In January 1988 for instance they reinforce each other to give a pronounced algebraic minimum, while in February 1988 the substantial minimum in the Rockies torque is largely compensated by the maximum in the Himalayas torque.

Figure 2

The atmospheric patterns associated with the IS mountain-torque variations are shown in Fig. 2. They are obtained by regressing the 700-hPa geopotential heights (Z_{700}) with respect to each mountain torque over the 40-year interval, all data being filtered to retain the IS band. East–west dipole patterns span the Rockies and the Himalayas, respectively, with their nodal lines located on the western (upwind) flanks of either mountain range. The amplitudes of the patterns in Figs. 2a and 2b are comparable, as expected from the fact that these two mountain ranges make comparable contributions to the NH mountain torque. The sum of the two dipoles essentially makes up the pattern constructed for the total NH T_M (see Fig. 2 of Part I).

b. Sectorial EOFs

To address the regional aspects of NH LFV and the potential influence of the separate mountain ranges on them, we carry out sectorial analyses along the same lines as the hemispheric analysis of empirical orthogonal functions (EOFs)

and torques presented in section 4 of Part I. The leading regional LFV patterns are determined by EOF analyses of the Pacific–North-American sector (120°E – 60°W ; PAC), the North-Atlantic–European sector (90°W – 90°E ; ATL) and the Eurasian sector (0°E – 180°E ; ASI).

To capture the dominant patterns of atmospheric variability, we compute the EOFs in each sector from 3-day mean 700-hPa geopotential maps over the 40-year record. EOF-1 for each of these sectors (not shown) is essentially of one (arbitrary) sign and represents the regional counterpart of the hemispheric EOF-1. Each sectorial EOF-1 describes changes in the midlatitude jet intensity that are associated primarily with the seasonal cycle (see Fig. 7a in Part I).

Over the Atlantic and Pacific sectors, EOF-2 represents changes in intensity of the midlatitude jet stream, as captured by NH EOF-2 (Fig. 7b in Part I): ATL EOF-2 (Fig. 3a) resembles the NAO (Van Loon and Rogers 1978), while PAC EOF-2 (not shown) has features in common with the West Pacific Oscillation (WPO) during winter months (Barnston and Livezey 1987).

Figure 3

The third EOF in each sector (PAC in Fig. 3b, and ASI in Fig. 3c) is wavetrain-like, with the dominant centers lying over the primary regions of high LFV: the Gulf of Alaska for the PAC sector and northern Scandinavia for the ASI sector. PAC EOF-3 (Fig. 3b) exhibits an east–west dipole with its N–S axis over the Canadian Rockies, while its strongest center of action is over the Gulf of Alaska. Its two opposite phases correspond to extension and contraction of the midlatitude jet over the eastern North Pacific; it is strongly reminiscent of Dole

and Black's (1990) Persistent North Pacific (PNP) pattern.

ASI EOF-3 (Fig. 3c) is an E–W dipole, having its strongest center of action over northern Scandinavia. It contains features of Wallace and Gutzler's (1981) East Atlantic pattern, and of Barnston and Livezey's (1987) Eurasian pattern, type 1. It is quite similar to the ATL EOF-3 (not shown), indicating the robustness of their common feature, the center of action over northern Scandinavia.

3 Rockies torque and regional LFV

Figure 4

The cross-spectra between the Rockies torque and the leading PAC PCs show significant peaks in the 20–30-day. For instance, in this frequency band, the cross-spectrum between the Rockies torque and PAC PC-3 (Fig. 4a), exhibits highly significant peaks: the two series are essentially in phase, with the torque slightly leading the changes in PC-3. This relationship follows from the fact that PAC EOF-3 (Fig. 3b) is dominated by large geopotential height variations across the Rockies that clearly entail a mountain torque. Another strong peak in the cross-spectrum with PC-3 is also present at 50–60 days, and is probably controlled by tropical oscillations, which do not concern us here.

Similar analyses indicate that in the 20–30-day band, the Rockies torque is in quadrature with the first PAC PC, and almost in quadrature with the second PC (not shown). The latter relationship is quite modest in amplitude, and only one peak at 23–24 days is significant in the cross-spectrum at the 99% level. There is

no strong correlation between the leading PCs (that is the PCs 1 to 3) over the ATL and ASI sectors and the Rockies torque.

To examine the lead-lag relationship between the Rockies torque and PAC PC-3 (Fig 4a), we filter the Rockies T_M series by using the 20–30-day bandpass filter introduced in section 3 of Part I. The band-passed series represents about 40% of the IS variance of the Rockies torque. The corresponding IS Z_{700} composites are shown in Fig. 5, which is computed in the same way as Fig. 5 of Part I, with a threshold value of 11.8 H for the 20–30-day Rockies T_M . With this value, $N_c = 80$ IS Z_{700} maps enter into each composite, the same number as used in the hemispheric Fig. 5. As in Part I, we have verified that our sectorial results here are not sensitive to moderate changes in the threshold.

Figure 5

At –3-day lag (Fig. 5a), the composite shows a strong SE–NW dipole, with a pronounced cyclonic anomaly along the western flank of the Rockies and an anticyclonic one centered over the Alaskan peninsula. The successive positive and negative anomaly centers downstream of the Rockies are indicative of the presence of Rossby lee waves. At 0-day lag (Fig. 5b), that is in phase with the extrema of the Rockies torque, the cyclonic anomaly located along the western flank of the Rockies has increased in size and intensity, and moved 5° northward. By this time, the downstream wave train has increased in amplitude, while the anticyclonic anomaly over Alaska has weakened and contracted considerably; the composite essentially reproduces the dipole pattern associated with a strong Rockies torque in Fig. 2a. As time increases further, the cyclonic pattern located upstream of

the Rockies starts to spread and move northwestward (Fig. 5c). It is at this time that the composite exhibits the largest correlation with PAC EOF-3 in Fig. 3b. The cyclonic pattern becomes centered near the Alaskan peninsula at 6-day lag, that is in approximate quadrature with the Rockies torque (Fig. 5d).

Figure 6

The evolution of the AAM budget, as keyed to the to 20–30-day Rockies torque, is displayed in Fig. 6. At –3-day lag, the AAM (grey dashed line in Fig. 6) is near 0. This indicates that the positive AAM associated with the southern flank of the cyclonic pattern located upstream of the Rockies in Fig. 5a is balanced by the negative AAM associated with the anticyclone centered over the northern Central Pacific. At 0-day lag, the cyclonic pattern amplifies, while the anticyclonic one decays, and the AAM becomes positive. Note that, because of earth’s sphericity, cyclonic anomaly patterns in mid-latitudes make a positive contribution to AAM, while the contribution of anticyclonic anomalies is negative. The composite AAM value at this time is near 25 Hd, which is moderate when compared to the AAM standard deviation of 100 Hd in the IS band but still significant at the 95% level, as indicated by the thick grey vertical bar in Fig. 6. Thereafter, the AAM increases to reach a maximum above 50 Hd at 3-day lag, when the cyclonic anomaly has extended to cover most of the northeastern Pacific. At 6-day lag, the AAM starts to decay; at this time the cyclonic anomaly has contracted in space, decreased in amplitude, and moved substantially northward.

The Rockies torque composite in the IS band (black solid in Fig. 6) also reaches substantial values when compared for instance with the NH mountain torque’s

standard deviation of $\sigma_T = 10$ H (see Part I). The integral of the IS Rockies torque (thick grey line in Fig. 6) agrees quite well in phase and amplitude with the IS AAM variations.

The curves in Fig. 6 suggest that the Rockies torque contributes to the changes in the eastern Pacific subtropical and midlatitude jets seen in the composite maps of Fig. 5. To support this suggestion more quantitatively, we have evaluated the contribution to the AAM from the anomaly patterns in Fig. 5, by retaining in the horizontal AAM integrals in Eqs. (3) and (5) of Part I only the contribution of the eastern midlatitude Pacific (120°W – 180°W , 20°N – 50°N). The evolution of the AAM evaluated over this sector and keyed to the 20–30-day Rockies torques (not shown) is almost exactly in phase with the composite evolution of the global IS AAM in Fig. 6, and about 3 times smaller in amplitude. This result remains valid if we take for the barotropic wind in Eq. (5) of Part I, and for the surface pressure P_s in Eq. (6) of Part I, the values derived from the maps in Fig. 5 by using geostrophy and hydrostatic equilibrium, respectively. The Rockies torque is thus easily large enough to drive the flow pattern changes in the eastern Pacific, between 20°N and 50°N , that are shown in Fig. 5.

Two additional items deserve attention here. The first is the presence of Rossby lee waves in Fig. 5, which supports the theory of Kalnay-Rivas and Merkin (1981), who attributed blocking onset over the North Atlantic to such waves. Unfortunately, the low correlations between the Rockies torque and the ATL PCs indicate that the circulation anomalies associated with the Rockies over the

Atlantic are too weak to correlate significantly with one of the leading Atlantic EOFs.

The second item is that, over the eastern Pacific, our coherent large-scale circulation patterns in Fig. 5 have some features in common with the 25-day oscillation found by Branstator (1987), Kushnir (1987), and Ghil and Mo (1991) using more direct methods. For instance, we note the northward and slightly westward displacement of the low that is located initially along the western flank of the Rockies in Fig. 5a and settles over the Alaskan peninsula 9 days later in Fig. 5d. This shift is reminiscent of the displacement of the low that starts off along the western flank of the Rockies in Fig. 11c of Kushnir (1987) and ends up slightly to the south of Alaska in Fig. 11e, 10 days later.

4 Himalayas torque and regional LFV

The cross-spectra between the Himalayas torque and the leading ASI PCs also show significant peaks in the 20–30-day band. Thus the cross-spectrum between the Himalayas torque and ASI PC-3 exhibits a highly significant peak near 20 days and 3 other less pronounced peaks in this band (Fig. 4b). In this frequency band, the two series are almost in phase, with PC-3 slightly leading the changes in the torque. The spatial pattern of ASI EOF-3 (Fig. 3c) shows that a positive PC-3 is associated with a pronounced low over Scandinavia. A negative anomaly of similar extent is associated, at zero lag, with a large Himalayas torque (Fig. 2b).

In the same band, the Himalayas torque is in quadrature with the first ASI PC (not shown), which characterizes changes in the midlatitude jet's intensity near the subtropics and over the western Pacific. Highly significant relationships are also found for ASI PC-2 (not shown).

In this band, a correlation exists, furthermore, between the Himalayas torque and ATL PC-2, which captures the evolution of the NAO; the torque and the PC are in quadrature (not shown). This lag correlation is only marginally significant, but suggests an upstream influence of the Himalayas on the NAO. It is consistent with the NH mountain torque and NH PC-2 being in quadrature (see Part I), because the Himalayas torque makes a substantial contribution to the NH torque and because ATL EOF-2 (the NAO) is the sectorial component of the NH EOF-2 (the Arctic Oscillation; see section 2b). The Himalayas also seem to have some downstream influence on the PAC EOF-1.

Figure 7

We analyze next the evolution of the Z_{700} geopotential fields during the 20–30-day cycle in the Himalayas torque to interpret these relationships. The composites in Fig. 7 use a threshold value for the 20–30-day Himalayas torque of 12 H. This value ensures again that $N_c = 80$ maps are selected.

At –6-day lag (Fig. 7a), the circulation is anticyclonic almost everywhere, with significant negative zonal wind anomalies in the subtropical Central Pacific and a weak midlatitude jet over the North-Atlantic sector. At –3-day lag, a positive Himalayas torque starts to build up, and the composite anomaly is dominated by an east–west dipole pattern whose N–S axis lies along the western flank of

the Tibetan Plateau (Fig. 7b). At that time, the negative zonal wind anomalies over the subtropical Pacific have significantly decreased compared to Fig. 7a. In phase with the Himalayas torque (Fig. 7c), the anomalies essentially present the dipole pattern along the western flank of the Tibetan Plateau that is responsible for the strong Himalayas torque in Fig. 2b. Elsewhere the circulation anomalies are rather weak, although a large-scale cyclonic monopole starts to cover the Pacific basin, consistent with the downstream propagation found by Weickmann et al. (2000).

At 3-day lag (Fig. 7d) the cyclonic part of the east–west dipole spreads westward and expands, so that the circulation becomes predominantly cyclonic over all of northern Europe. A cyclonic monopole now covers the Pacific basin, where it is associated with enhanced subtropical zonal winds. At 6-day lag (not shown but the map is very similar to Fig. 7a with the sign reversed), the cyclonic anomaly that covers the Pacific basin is almost unchanged, while the cyclonic monopole that covers northern Europe in Fig. 7d splits into two cyclonic monopoles, one centered slightly east of Greenland, the other over western Siberia.

Figure 8

The composite evolution of the AAM budget in the IS band, as keyed to the evolution of the 20–30-day Himalayas torque, is plotted in Fig. 8. The AAM itself (dashed grey) exhibits even more substantial and significant variations than over the 20–30-day cycle in Rockies torque (Fig. 6). Furthermore, large and positive values of the AAM at +3-day and +6-day lag in Fig. 8 correspond to an enhanced subtropical jet over the Central Pacific, and an enhanced midlatitude Atlantic

jet (see Fig. 7d but also Fig. 7a with the sign reversed). The composite of the Himalayas torque (black solid in Fig. 8) exhibits substantial and significant values as well. Its integral in time (grey solid) closely follows the composite evolution of the AAM.

The results in Fig. 8 suggest that the Himalayas torque plays a substantial role in affecting the flow patterns in the subtropical Pacific and in the northern Atlantic that appear in Fig. 7. We have verified quantitatively this point by looking at the contribution of these two sectors to the global AAM in the IS band. AAM composites of either sector (not shown) are almost in phase with and substantially smaller than the global AAM composites in Fig. 8. This result again stays valid if the sectorial contributions to M are evaluated directly from the Z_{700} composite maps, using the geostrophic and hydrostatic balances. The Himalayas torque can thus easily account for the corresponding changes in both sectors.

The composites patterns over the Euro-Atlantic sector in Fig. 7 are strongly reminiscent of the NAO cycles that have been found in previous studies, near the frequency band of interest here. Over the North Atlantic and Europe, the maps in Figs. 7a–7d match well the composite maps in Figs. 10a–10d of Plaut and Vautard (1994), with the sign reversed; the latter describe half a cycle of the 30–35-day oscillation that dominates NAO variability from time to time. This oscillation is characterized by the retrogression of a dipole pattern from northeastern Europe toward the North Atlantic, as seen in our Figs. 7c and 7d.

5 Mountain torques and winter circulation regimes

LFV is often better described in terms of persistent flow patterns that have no preferred duration and whose onset and decay can be quite abrupt (Ghil 1987; Ghil and Robertson 2002; Koo et al. 2002). The oscillatory description in Part I and in sections 3, 4, and 5 above may underestimate, therefore, the relationships between mountain torques and LFV. This can be the case if the different series are only related episodically.

To establish statistically if such episodic links can be recognized, we next proceed with a regime classification based on the centroids of the Pacific and Atlantic sectorial regimes identified by Smyth et al. (1999), using a Gaussian mixture model. Their two Atlantic regimes resemble contrasting phases of the NAO pattern; hence we take the positive polarity of ATL EOF-2 in Fig. 3a as the first ATL regime centroid, and its negative polarity as the second one. These two regimes thus correspond to high and low NAO index, respectively (Hurrell 1995). The two Pacific regimes of Smyth et al. (1999) resemble contrasting phases of the PNP pattern, and hence of our PAC EOF-3 (Fig. 3b); thus we take PAC EOF-3 as the first PAC regime centroid, and minus PAC EOF-3 as the second one. Our two PAC regimes thus correspond to high- and low-index flow over this ocean basin (Namias 1950).

As in Mo and Ghil (1987, 1988) and Kimoto and Ghil (1993b), we use pattern correlation as the measure of distance between a given map and a regime centroid.

We identify regime *episodes* as the individual 3-day mean maps whose pattern correlation with the corresponding centroid is greater than a given threshold; the date of the episode is the middle one of the three days over which the map is computed. We identify regime *events* to be the episodes that persist 6 days or longer without interruption. The *onset* of a given event is then taken as its first day and its *break* as its last day. For the 40 years of our dataset, we have chosen a pattern correlation threshold of 0.75; with this value, 50 to 70 episodes and 20 to 30 events are obtained for each of the four regimes described above.

To establish relationships between mountain torques and weather regimes, we first computed, for each mountain torque T_M and for each weather regime episode E , the probability that T_M is positive at a time t counted from the date of E ,

$$P(T_M > 0 \text{ at } t \text{ after } E). \quad (1)$$

In all cases, and except when specified, the torque T_M in Eq. (1) was taken from the IS (10–150-day) series of torques: NH, Rockies or Himalayas.

a. Atlantic regimes and mountain torques

For the Atlantic sector, the probabilities of Eq. (1) show that Atlantic Regime-1 episodes have a reduced probability (35% at 3-day lag) to be followed by a positive NH torque, while Regime-2 episodes have an enhanced probability (near 75% at 3-day lag) to be followed by a positive NH torque. To synthesize these findings, and further test their statistical significance, we next combined them and evaluated the probability P_{ATL} , for NH mountain torque T_M with respect to

ATL regimes,

$$P_{ATL} = P(\{T_M > 0 \text{ at } t \text{ after } E_1\} \text{ or } \{T_M < 0 \text{ at } t \text{ after } E_2\}). \quad (2)$$

Table 1

The results that are significant at the 99%-level are displayed in the Table 1; the statistical significance is estimated using a Monte Carlo procedure in which the computed probabilities are compared to an ensemble of probabilities computed with the same series and episodes but with randomly chosen lag. This test typically establishes that probabilities between 40% and 60% are not significant. These two values bracket $P_{ATL} = 50\%$, the expected result when the sign of the torque is entirely independent of the atmospheric circulation pattern and lag considered in Eq. (2).

The first row in Table 1 shows that there is significantly reduced probability that the NH mountain torque is positive 0, 3 and 6 days after episodes in Regime 1 and negative after episodes in Regime 2. The second row reports the analysis results for the 20–30-day T_M signal analyzed in Sections 3 and 4 of Part I. It also shows very significant probabilities at the same lags, indicating that the 20–30-day NH torque variations described in Part I are important in the episodic context as well. The third and fourth rows present the same statistics but using the intraseasonal Rockies and Himalayas torques, respectively. They show that only the Himalayas torque can be related to the ATL regime episodes at the 99% level, consistent with Fig. 7.

In ATL Regime 1, PC-2 is positive and the midlatitude jet intensity is larger than usual, while in Regime 2, PC-2 is positive and the jet intensity is reduced. This finding, plus the fact that the probabilities in Table 1 are only significant at zero and small positive lag after regimes episodes, suggest that the breaks of Regime-1 events result, at least in part, from a brief deceleration of the westerly jet due to a negative NH mountain torque anomaly. Conversely, the breaks of Regime-2 events result, at least in part, from a brief acceleration due to a positive NH mountain torque anomaly.

Following this interpretation, we computed the probability that the NH mountain torque in the IS band is negative during the breaks of Regime-1 events and positive during the breaks of Regime-2 events. This probability is close to 80%, and highly significant; it still equals 77% if one tests the sign of the NH mountain torque in this band 3 days after the regime event breaks. Testing the sign of the IS Himalayas torque results in a probability of 70% during the regime event breaks.

b. Pacific regimes and mountain torques

To check if mountain torques are related to the PAC regimes as well, we computed the probability that the mountain torque is positive after a Pacific regime episode. In more than 70% of cases, episodes in PAC Regime 1 are preceded for a few days ($t = -6, -3$ and 0 day) by a positive torque. Conversely, in less than 35% of cases the episodes in PAC Regime 2 are preceded for a few

days ($t = -6$ and -3 days) by a positive torque.

Table 2

We evaluated again the combined probability P_{PAC} of the two types of circumstances,

$$P_{PAC} = P(\{T_M > 0 \text{ at } t \text{ after } E_1\} \text{ or } \{T_M < 0 \text{ at } t \text{ after } E_2\}). \quad (3)$$

The most highly significant results are shown in Table 2. Row 1 indicates that a strong IS signal in NH mountain torque precedes the Pacific regime episodes at 3, 6 and 9 days. Row 2 confirms that this lead-lag relationship in the IS band largely results from the 20–30-day signal described in Part I. In this narrower band, a very significant NH T_M signal is present even 15 days prior to the PAC regime episodes. The last two rows in Table 2 show that the above results are not much modified if one considers the Rockies torque only. This finding indicates that the links between PAC regimes and the mountain torques result from an upstream influence of the Rockies (cf. Fig. 5).

That the mountain torque changes precede the PAC regime episodes suggests that the former can be related to the onset of PAC regime events. To address this point we next computed the probability that the mountain torque is positive at the onset of events in PAC Regime 1 and negative at the onset of events in PAC Regime 2. When computed for the NH torque in the IS band, this probability is close to 84%. If the torque value is taken 3 days prior to a PAC regime onset, the probability of the torque having the appropriate sign is still 80%. Again, these links result primarily from an upstream influence of the Rockies, as the two

probabilities above are 69% and 77% when evaluated using the Rockies torque in this band.

6 Concluding remarks

The NH mountain torque variations described in Part I of this study (Lott et al. 2003) are often associated, in the 20–30-day band, with highly regional circulation patterns (see Fig. 2 of Part I and Figs. 2a, b here). Moreover, the contribution of the Rockies and Himalayas to the NH mountain torque T_M , while jointly making up 85% of the variance in the latter, are largely independent of each other (see Fig. 1 here and its discussion in section 2a). These two facts motivate our regional analysis in the present Part II.

This analysis used three partially overlapping sectors which we dubbed ATL (90°W–90°E), ASI (0°E–180°E), and PAC (120°E–60°W). A spectral analysis of the relationships between regional mountain torques and the dominant patterns of sectorial LFV identified clear signals in the 20–30-day band (Fig. 4). These dominant patterns were obtained by principal component (PC) analysis of year-round low-frequency variability (LFV).

At small lag, the Rockies torque is significantly related to PAC EOF-3 variability and the Himalayas torque is related to EOFs 2 and 3 of ASI LFV. These three regional LFV patterns are naturally associated with a mountain torque because they are strongly nonzonal and centered upstream of the Rockies, for

PAC EOF-3, and the Tibetan Plateau, for the Asian EOFs 2 and 3. When the atmospheric circulation locally resembles one of these patterns, the associated zonal pressure gradients across the corresponding mountain range are large, and result in a substantial torque. These patterns exhibit, therefore, lag relationships of near-simultaneity with the appropriate regional mountain torque; the torque tends, nevertheless, to lead PAC PC-3 by a few days (see Fig. 4 and its discussion in section 3a).

As in our hemispheric analysis (Part I), there are also dominant regional LFV patterns that do not exhibit substantial pressure gradients across the major mountain ranges. These patterns include all three first-ranked regional EOFs as well as the second-ranked EOFs, that is the West Pacific Oscillation and the NAO in our analysis. Each of these patterns is predominantly zonal in character and thus does not give rise to a mountain torque, in and of itself. The torques lead these zonal patterns by nearly one-quarter period in the 20–30-day band, which suggests that the former drive the changes in the latter.

The atmospheric flow field composites that accompany the 20–30-day mountain torques allow us to understand these relationships. Over the northeastern Pacific and North America, as well as the northeastern Atlantic and Europe, these composites resemble the atmospheric oscillations that dominate NH LFV from time to time, as found in previous studies (Branstator 1987; Kushnir 1987; Ghil and Mo 1991; Plaut and Vautard 1994). During these oscillations, and apparently in response to the regional torques (the Rockies torque for Fig. 5 and the

Himalayas torque for Fig. 7) substantial AAM changes do occur in the IS (10–150-day) band. For the Rockies torque, these AAM changes can be attributed directly to the flow patterns in the midlatitude eastern Pacific (see Fig. 5).

Accordingly, the Rockies torque is large enough to drive, at least to a substantial degree, the changes in the midlatitude jet seen in these maps. The same analysis for the Himalayas torque shows that the latter can drive the changes in the subtropical Pacific and in the midlatitude North Atlantic seen in the composite maps of Fig. 7.

We have also investigated systematically to what extent the regional results here are related to the hemispheric ones in Part I. We found for instance that the Himalayas and the Rockies torque are both linked with the NH EOF-1. The Himalayas' contribution is nevertheless larger than that of the Rockies. The Himalayas T_M also leads the NH EOF-2, by about a quarter of a period, but we found no significant link between the Rockies torque and NH EOF-2.

Conversely, we found highly significant links between the hemispheric T_M and the regional EOFs (not shown). These links imply that the changes in the NH T_M are related to substantial circulation anomalies in all three sectors. The most striking relationship is between the hemispheric torque and PAC PC-3; the links between the Rockies torque and PAC PC-3 presented in section 3a here are at the basis of this relationship. Likewise, we find links between the NH mountain torque (not shown) and ATL PC-2, based on the relationship between the Himalayas torque and ATL PC-2, mentioned in section 4a.

It is also instructive to compare the composite maps in Figs. 5 and 7 with the composite maps in Fig. 5 of Part I. Doing so shows that the atmospheric flow field variations associated with the 20–30-day NH T_M (see Fig. 5 of Part I) are essentially associated with the Himalayas torque: except near the Rockies, the composite maps in Fig. 5 of Part I are very similar to those associated with the Himalayas torque in Fig. 7 here.

This comparison also helps to interpret the westward development of the large-scale cyclonic anomaly that covers the whole Pacific basin, in near quadrature with the 20–30-day NH torque (Figs. 5b and 5c in Part I). When the two regional torques vary in phase to give a significant 20–30-day NH T_M , the patterns associated with each of them in Figs. 5 and 7 here reinforce each other. The cyclonic pattern lying to the west of the Rockies at 0-day lag in Fig. 5a of Part I corresponds to that associated with the Rockies torque at the same lag (Fig. 5b here). The strong extension toward the west of this pattern 3 days later (Fig. 5b of Part I), results from the fact that the cyclonic pattern associated with the Rockies torque has spread toward the northwest at that time (Fig. 5c here) and from the fact that the Himalayas torque is also associated with a large-scale cyclonic pattern over the central North Pacific at the same time (Fig. 7d here).

Complementing this description of sectorial LFV, we also carried out an investigation of sectorial regimes. To do so, we relied on the previous work of Smyth et al. (1999) and chose our regimes centroids to coincide with theirs, which in turn resemble those of Cheng and Wallace (1993; see also Ghil and Roberstson 2002).

These centroids correspond essentially to opposite polarities of the NAO and PNP patterns, in the Atlantic and the Pacific sector respectively. Our regimes thus represent the persistent, quasi-stationary flow configurations that characterize, from time to time, the large-scale flow in the midlatitudes.

We found a significant signal in the intraseasonal NH mountain torque during the breaks of the two Atlantic regimes that resemble opposite phases of the NAO: a negative torque at the end of the zonal-flow events, and a positive torque at the end of the blocked-flow events. This effect is primarily due to the Himalayas torque (see Table 1). As blocked-flow events are associated with reduced jet intensity, we found here here that a process that tends to augment AAM can help end blocking. Conversely, it is not surprising to find that a process that tends to reduce AAM can help end a zonal-flow event, characterized by an intense jet.

We found, moreover, a signal in the NH mountain torque during the onset of the two PAC regimes: a positive one at the beginning of zonal-flow events, and a negative torque at the beginning of blocked-flow events. This precursor signal is primarily due to the Rockies torque (see Table 2). Again, as the Rockies torque enhances AAM, it is not surprising to find a positive torque preceding zonal-flow events, and a negative torque preceding blocked-flow events, which are associated with a strong as opposed to a weak jet over the eastern Pacific.

To determine if the 20–30-day mountain torques are in part responsible for the above transitions, we repeated the statistical estimates of Tables 1 and 2 using the 20–30-day mountain torque signals, constructed with the 20–30-day

band-pass filter used in Part I. The relationships between mountain torques and flow regimes in this band (see again Tables 1 and 2) indicate that the 20–30-day signals participate significantly in the flow regime transitions. The predictive value of these lead-lag relationships between mountain torques and large-scale sectorial flow patterns, if any (Lott et al. 2001; Ghil and Robertson 2002; Koo et al. 2002), remains to be evaluated.

Acknowledgments

The authors are grateful to past and present associates on three continents for interesting exchanges on low-frequency atmospheric variability. The NCEP/NCAR Reanalysis data are provided through the NOAA Climate Diagnostics Center (<http://www.cdc.noaa.gov>). Extensive and persistent comments by Klaus M. Weickmann and two anonymous referees have greatly improved the presentation of our results. This work was supported by NASA grant NAG5-9294 (F.L.), DOE grant DE-FG03-01ER63260 (A.W.R.) and NSF grant ATM-0082131 (M.G.).

References

- Barnston, A. G. and R. E. Livezey, 1987: Classification, seasonality and persistence of low-frequency atmospheric circulation patterns, *M. Weath. Rev.*, **115**, 1083–1126.
- Blackmon, M. L., Y.-H. Lee and J. M. Wallace, 1984: Horizontal structure of 500 mb height fluctuations with long, intermediate and short scales, *J. Atmos. Sci.*, **41**, 961-979.
- Cheng, X., and J. M. Wallace, 1993: Cluster analysis of the northern hemisphere wintertime 500-hPa height field: spatial patterns, *J. Atmos. Sci.*, **50**, 2674–2696.
- Dickey, J. O., M. Ghil, and S. L. Marcus, 1991: Extratropical aspects of the 40-50 day oscillation in length-of-day and atmospheric angular momentum, *J. Geophys. Res.*, **96**, 22643–22658.
- Dole, R. M., and N. M. Gordon, 1983: Persistent anomalies of the extratropical Northern Hemisphere winter time circulation: geographical distribution and regional persistence characteristics, *Mon. Wea. Rev.*, **111**, 1567–1586.
- Dole, R. M., and R. X. Black, 1990: Life cycle of persistent anomalies. Part II: The development of persistent negative height anomalies over the North Pacific Ocean, *Mon. Wea. Rev.*, **111**, 824–846.
- Ghil, M., 1987: Dynamics, statistics and predictability of planetary flow regimes, in *Irreversible Phenomena and Dynamical Systems Analysis in the Geo-*

- sciences*, C. Nicolis and G. Nicolis (Editors), D. Reidel, Dordrecht/Boston/Lancaster, 241–283.
- Ghil, M., and K.-C. Mo, 1991: Intraseasonal oscillations in the global atmosphere. Part I: Northern Hemisphere and tropics, *J. Atmos. Sci.*, **48**, 752–779.
- Ghil, M., and A. W. Robertson, 2002: Waves vs. particles in the atmosphere's phase space: A pathway to long-range forecasting?, *Proc. Natl. Acad. Sci.*, **99 (Suppl. 1)**, 2493–2500.
- Ghil, M., M. Kimoto, and J. D. Neelin, 1991a: Nonlinear dynamics and predictability in the atmospheric sciences, *Rev. Geophys.*, Supplement (U.S. Nat'l Rept. to Int'l Union of Geodesy and Geophys. 1987–1990), **29**, 46–55.
- Ghil, M., S. L. Marcus, J. O. Dickey, and C. L. Keppenne, 1991b: AAM the Movie. NTSC Videocassette AVC-91-063, Caltech/NASA Jet Propulsion Laboratory, Pasadena, CA 91109 [available also from MG upon request].
- Higgins, R. W., and K. C. Mo, 1997: Persistent North Pacific Circulation anomalies and the tropical intraseasonal oscillation, *J. Climate*, **10**, 223–244.
- Hoskins, B. J., and D. J. Karoly, 1981: The steady linear response of a spherical atmosphere to thermal and orographic forcing, *J. Atmos. Sci.*, **38**, 1179–1196.
- Hoskins, B. J., and P. J. Valdes, 1990: On the existence of storm tracks, *J. Atmos. Sci.*, **47**, 1855–1864.

- Hurrell, J. W., 1995: Decadal trends in the North Atlantic Oscillation regional temperatures and precipitation, *Science*, **269**, 676–679.
- Kalnay-Rivas, E., and L. O. Merkin, 1981: A simple mechanism for blocking, *J. Atmos. Sci.*, **38**, 2077–2091.
- Keppenne, C. L. and M. Ghil, 1993: Adaptive filtering and prediction of noisy multivariate signals: An application to subannual variability in atmospheric angular momentum, *Intl. J. Bifurcation Chaos*, **3**, 625–634.
- Kimoto, M., and M. Ghil, 1993a: Multiple flow regimes in the Northern Hemisphere winter. Part I: Methodology and hemispheric regimes, *J. Atmos. Sci.*, **50**, 2625–2643.
- Kimoto, M., and M. Ghil, 1993b: Multiple flow regimes in the Northern Hemisphere winter. Part II: Sectorial regimes and preferred transitions, *J. Atmos. Sci.*, **50**, 2645–2673.
- Koo, S., A. W. Robertson, and M. Ghil, 2002: Multiple regimes and low-frequency oscillations in the Southern Hemisphere’s zonal-mean flow, *J. Geophys. Res.*, pp. **A14** 14.1–14.13, 10.1029/2001JD001353.
- Lejenäs, H., and R. A. Madden, 2000: Mountain torques caused by normal-mode global Rossby waves, and the impact on atmospheric angular momentum, *J. Atmos. Sci.*, **57**, 1045–1051.
- Lott, F., 1999: Alleviation of stationary biases in a GCM through a mountain drag parameterization scheme and a simple representation of mountain lift

- forces, *Mon. Wea. Rev.*, **127**, 788–801.
- Lott, F., A. W. Robertson, and M. Ghil, 2001: Mountain torques and atmospheric oscillations, *Geophys. Res. Lett.*, **28**, 1207-1210.
- Lott, F., A. W. Robertson, and M. Ghil, 2003: Mountain torques and Northern-Hemisphere low-frequency variability Part I: Hemispheric aspects, *J. Atmos. Sci.*, *subjudice*.
- Marcus, S. L., M. Ghil, and J. O. Dickey, 1996: The extratropical 40-day oscillation in the UCLA general circulation model. Part II: Spatial structure, *J. Atmos. Sci.*, **53**, 1993–2014.
- Mo, K., and M. Ghil, 1987: Statistics and dynamics of persistent anomalies, *J. Atmos. Sci.*, **44**, 877–901.
- Mo, K., and M. Ghil, 1988: Cluster analysis of multiple planetary flow regimes, *J. Geophys. Res.*, **93D**, 10927–10952.
- Molteni, F., A. Sutera, and N. Tronsi, 1988: The EOFs of the geopotential eddies at 500 mb in winter and their probability density distributions, *J. Atmos. Sci.*, **45**, 3063–3080.
- Molteni, F., S. Tibaldi, and T. Palmer, 1990: Regimes in the wintertime circulation over northern extratropics. 1: Observational evidence, *J. Atmos. Sci.*, **47**, 31–67.
- Namias, J., 1950: The index cycle and its role in the general circulation, *J. Meteorol.*, **7**, 130-139.

- Penland, C., M. Ghil, and K. M. Weickmann, 1991: Adaptive filtering and maximum entropy spectra with application to changes in atmospheric angular momentum, *J. Geophys. Res.*, **96**, 22,659–22,671.
- Plaut, G., and R. Vautard, 1994: Spells of low-frequency oscillations and weather regimes in the northern hemisphere, *J. Atmos. Sci.*, **51**, 210–236.
- Rogers, J. C., 1981: The North-Pacific Oscillation, *J. Climatol.*, **1**, 39–57.
- Smyth, P., K. Ide, and M. Ghil, 1999: Multiple regimes in northern hemisphere height fields via mixture model clustering, *J. Atmos. Sci.*, **56**, 3704–3723.
- Van Loon, H., and J. C. Rogers, 1978: The seesaw in winter temperature between Greenland and Northern Europe. Part I: General description, *Mon. Wea. Rev.*, **106**, 296–310.
- Vautard, R., K. C. Mo, and M. Ghil, 1990: Statistical significance test for transition matrices of atmospheric Markov chains, *J. Atmos. Sci.*, **47**, 1926–1931.
- Wallace, J. M., and D. S. Gutzler, 1981: Teleconnections in the geopotential height field during the northern hemisphere winter, *Mon. Wea. Rev.*, **109**, 784–812.
- Weickmann, K. M., W. A. Robinson, and C. Penland, 2000: Stochastic and oscillatory forcing of global atmospheric angular momentum, *J. Geophys. Res.*, **105**, D12, 15543–15557.

	$t(\text{days})$					
	T_M leads			E leads		
	-6	-3	0	3	6	9
IS NH T_M			33	30	34	
20-30-d NH T_M			38	32	38	
IS Roc. T_M						
20-30-d Roc. T_M						
IS Him. T_M			39	36	35	
20-30-d Him. T_M	61			39	40	

Table 1: Probability (in percent) that a mountain torque T_M (left column) is either positive t days after an episode E of ATL Regime 1 or negative t days after an episode E of ATL Regime 2. IS stands for the intraseasonal, 10–150-day band; 20–30-d stands for the series filtered by the 20–30-day band-pass filter displayed in Fig. 4b of Part I. Only values significant at the 99% level are displayed.

	$t(\text{days})$						
	T_M	leads			E	leads	
	-15	-6	-3	0	3	6	9
IS NH T_M		66	74	66			39
20-30-d NH T_M		65	71	61		35	32
IS Roc. T_M		71	79	67			
20-30-d Roc. T_M	37	68	69	61		37	37
IS Him. T_M							
20-30-d Him. T_M							

Table 2: Probability (in percent) that a mountain torque T_M (left column) is either positive t days after an episode E of PAC Regime 1 or negative t days after an episode E of PAC Regime 2. Same conventions and parameters as in Table 1.

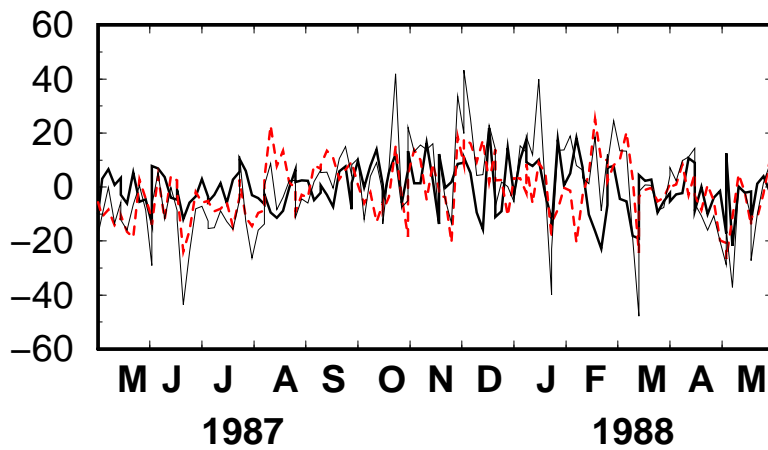


Figure 1: Northern Hemisphere (NH) mountain torque (light solid) and mountain torques due to the Rockies (heavy solid) and the Himalayas (dashed).

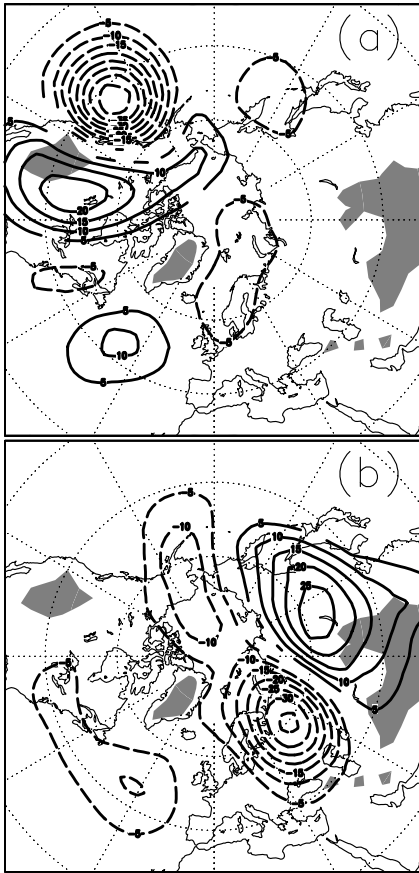


Figure 2: 700-hPa geopotential height field regression with respect to the mountain torque of the (a) Rockies and (b) Himalayas in the intraseasonal (IS) band; altitudes above 1500 m shaded. Positive contours are solid, negative ones are dashed; contour interval is 5 m. See Fig. 2 in Part I for the regression with respect to the total NH mountain torque.

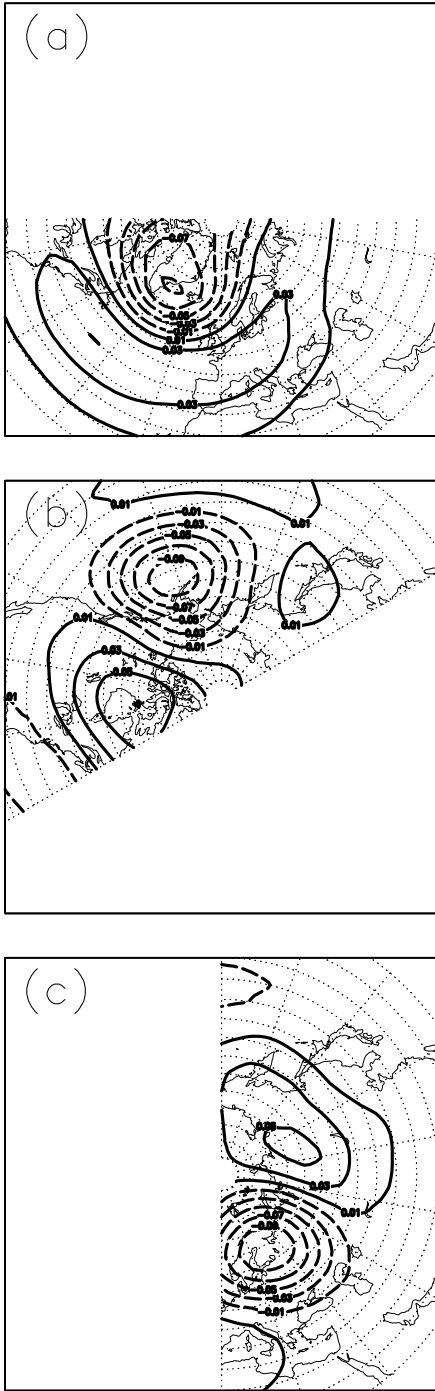


Figure 3: Selected regional EOFs of the 700-hPa geopotential heights: (a) ATL EOF-2; (b) PAC EOF-3; and (c) ASI EOF-3.

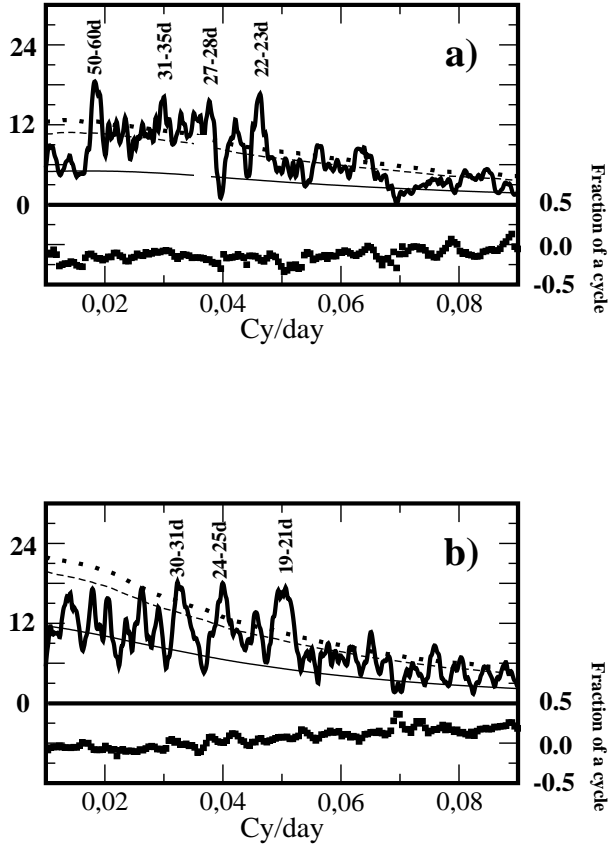


Figure 4: a) Cross-spectra between regional torques and sectorial PCs: a) Rockies T_M vs. PAC PC-3; and b) Himalayas T_M vs. ASI PC-3. Same conventions, parameters and methods as in Fig. 8 of Part I. Upper panels in (a) and (b): cross-spectral amplitude (thick solid) with 99% confidence level (heavy dots), 95% confidence level (light dashes), and median (light solid) of Monte-Carlo test; lower panels in (a) and (b): phase difference (filled squares).

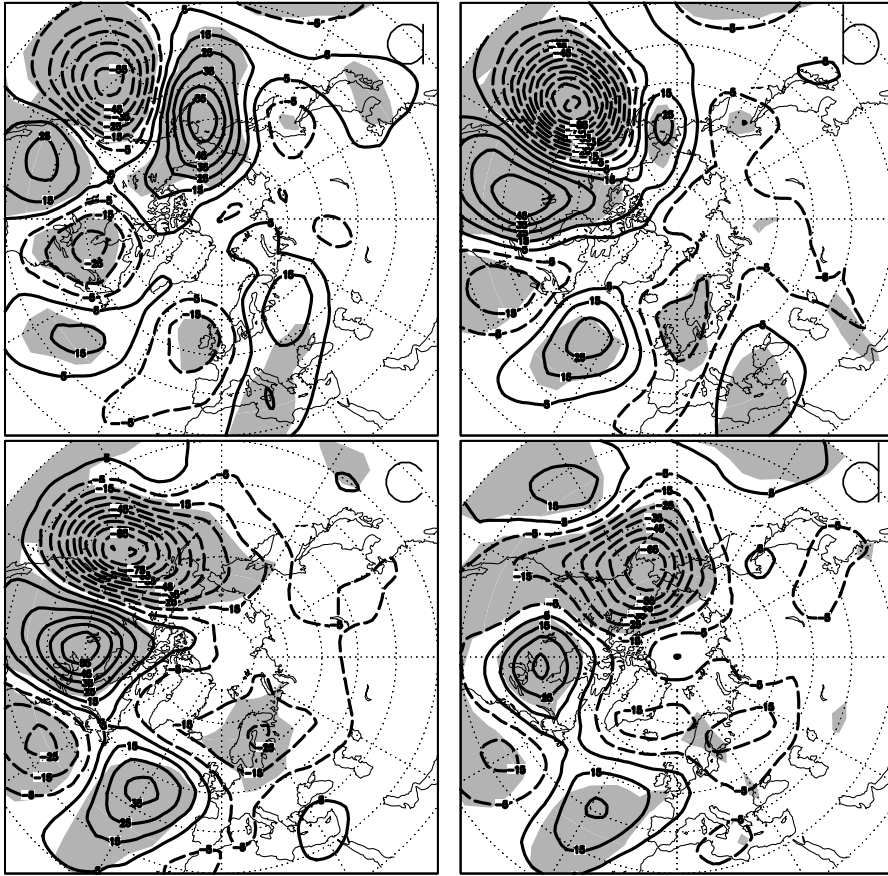


Figure 5: Composite anomalies of Z_{700} maps from the IS time series, keyed to the 20–30-day signal of the Rockies mountain torque: (a) –3-day lag; (b) 0-day lag; (c) 3-day lag; and (d) 6-day lag. Same procedure, conventions and parameters as in Fig. 5 of Part I.

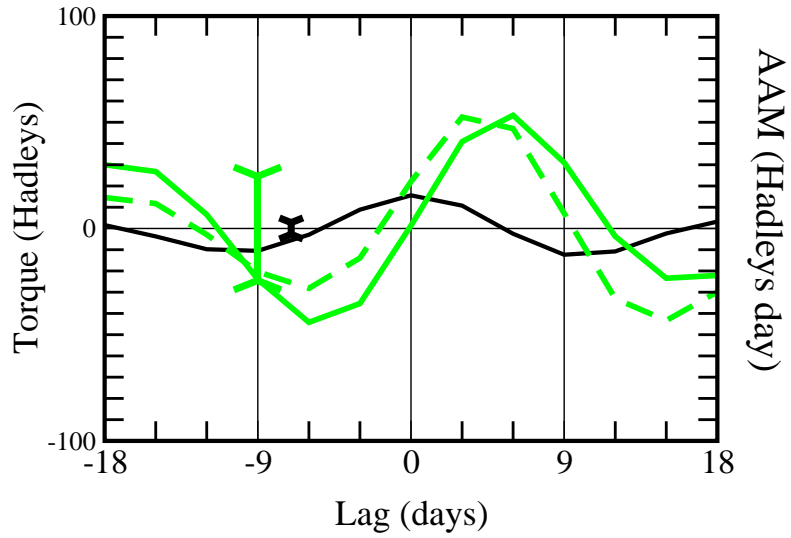


Figure 6: Composites of different terms in the AAM budget during the composite cycle illustrated in Fig. 5: IS Rockies torque (black solid); integral of IS Rockies torque (grey solid); and global IS M (grey dashed). Same conventions and parameters as in Fig. 6 of Part I

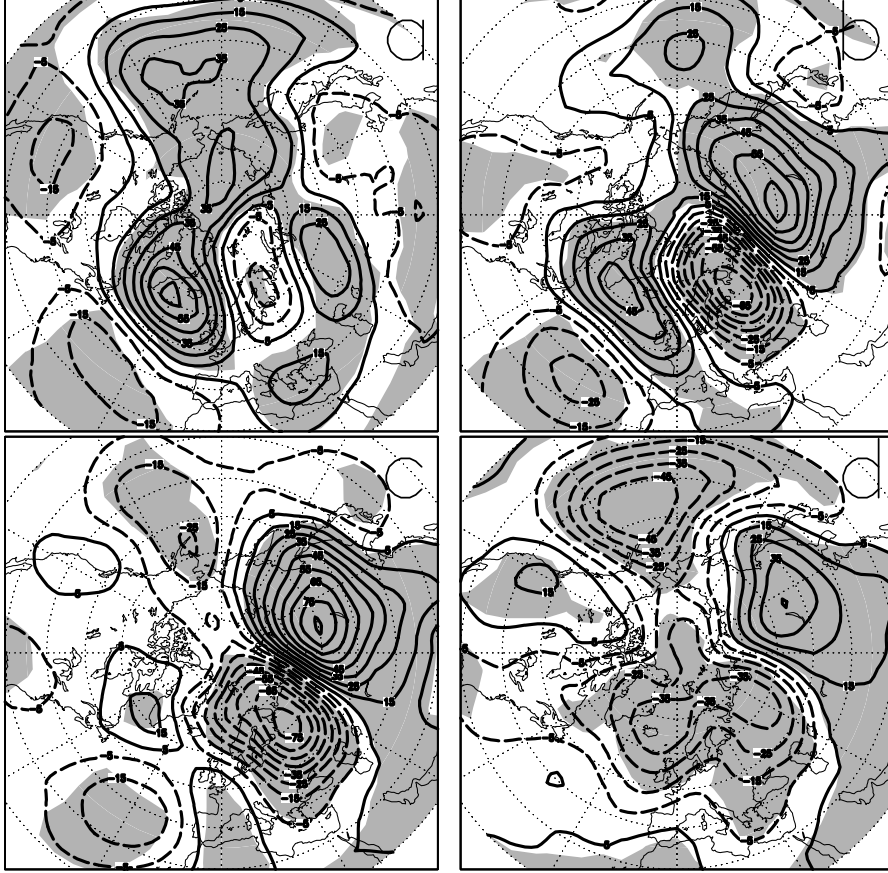


Figure 7: Composite anomalies of Z_{700} maps from the IS time series, keyed to the 20–30-day Himalayas mountain torque: (a) –6-day lag; (b) –3-day lag; (c) 0-day lag; and (d) 3-day lag. Same procedure, conventions and parameters as in Fig. 5 of Part I.

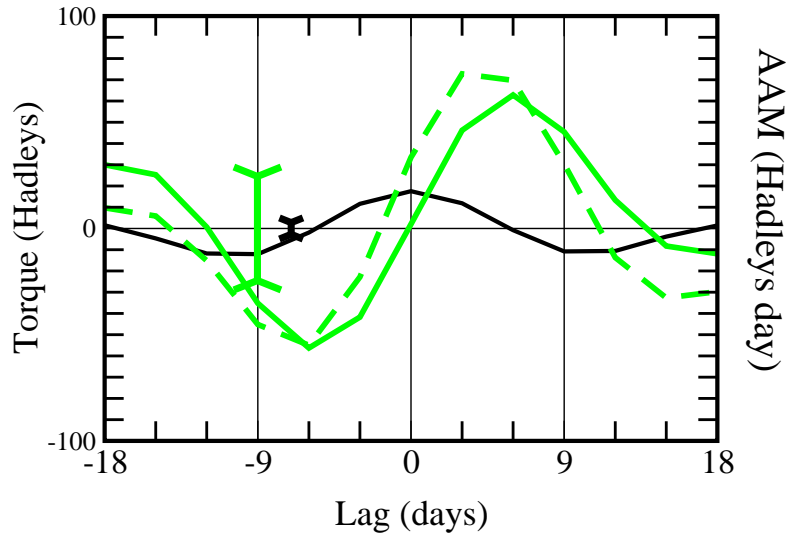


Figure 8: Composites of different terms in the AAM budget during the composite cycle illustrated in Figs. 7: IS Himalayas torque (black solid); integral of IS Himalayas torque (grey solid); and global IS M (grey dashed). Same conventions and parameters as in Fig. 6 of Part I.